CLINICAL INVESTIGATIVE STUDY

Objective biomarkers of depression: A study of Granger causality and wavelet coherence in resting-state fMRI

Ramona Cîrstian[1] | Jesper Pilmeyer[1,6] | Antoine Bernas[2] |
Jacobus F. A. Jansen[1,3] | Marcel Breeuwer[4] | Albert P. Aldenkamp[1,5] |
Svitlana Zinger[1,6]

[1]Department of Electrical Engineering, Eindhoven University of Technology, Eindhoven, The Netherlands

[2]Department of Biophysics, Radboud University Nijmegen, Nijmegen, The Netherlands

[3]Department of Radiology, Maastricht University Medical Center, Maastricht, The Netherlands

[4]Department of Biomedical Engineering, Eindhoven University of Technology, Eindhoven, The Netherlands

[5]Department of Neurology, Maastricht University Medical Center, Maastricht, The Netherlands

[6]Department of Research and Development, Epilepsy Center Kempenhaeghe, Heeze, The Netherlands

Correspondence
Jesper Pilmeyer, Department of Electrical Engineering, Eindhoven University of Technology, De Groene Loper 19, Flux, 5612 AP Eindhoven, The Netherlands.
Email: j.pilmeyer@tue.nl

Abstract

Background and Purpose: The lack of a robust diagnostic biomarker makes understanding depression from a neurobiological standpoint an important goal, especially in the context of brain imaging.

Methods: In this study, we aim to create novel image-based features for objective diagnosis of depression. Resting-state network time series are used to investigate neurodynamics with the help of wavelet coherence and Granger causality (G-causality). Three new features are introduced: total wavelet coherence, wavelet lead coherence, and wavelet coherence blob analysis. The fourth feature, pair-wise conditional G-causality, is used to establish the causality between resting-state networks. We use the proposed features to classify depression in adult subjects.

Results: We obtained an accuracy of 86% in the wavelet lead coherence, 80% in Granger causality, and 86% in wavelet coherence blob analysis. Subjects with depression showed hyperconnectivity between the dorsal attention network and the auditory network as well as between the posterior default mode network and the dorsal attention network. Hypoconnectivity was found between the anterior default mode network and the auditory network as well as the right frontoparietal network and the lateral visual network. An abnormal co-activation pattern was found between cerebellum and the lateral motor network according to the wavelet coherence blob analysis.

Conclusion: Based on abnormal functional dynamics between brain networks, we were able to identify subjects with depression with high accuracy. The findings of this study contribute to the understanding of the impaired emotional and attention processing associated with depression, as well as decreased motor activity.

KEYWORDS
causality, depression, fMRI, neurodynamics, resting-state networks, wavelet coherence

INTRODUCTION

Depression is a highly prevalent neuropsychiatric disorder and is characterized by depressed mood (feeling sad, empty), loss of interest and pleasure, sleep disturbances (insomnia or hypersomnia), fatigue, and feelings of worthlessness and guilt.[1] Currently, it is diagnosed based on symptomatic criteria, making the diagnosis of depression highly subjective. Up until now, there are no objective diagnostic tests available.[2]

Objective biomarkers of depression can help to improve the selection of particular treatments and constitute a step further toward personalized medicine. One of the most widely used brain imaging techniques is functional magnetic resonance imaging (fMRI). Resting-state functional MRI (rs-fMRI) is sensitive to blood-oxygenation level changes in the brain while the subject performs no particular task. These changes in blood oxygenation are indirectly associated with neural activity and therefore reflect brain activity alterations over time.

Brain connectivity refers to the idea that the brain is a network consisting of different regions or networks that are involved in executing one or more tasks. Effective connectivity is concerned with the influence of one neuronal system over another.[3–5] Functional connectivity (FC) represents the temporal correlation between different brain regions or networks, reflecting synchronous activation and has been an important topic among rs-fMRI studies in the recent years.[6–9] Quantitative analyses of rs-fMRI have shown that depressed subjects exhibit network abnormalities.[10,11]

Hu et al. used a deep learning-based Granger causality (G-causality) estimator on rs-fMRI and structural MRI data to identify subjects with Alzheimer's disease using a support vector machine (SVM) classifier, yielding an accuracy of up to 91.49%.[12] In another study by Luo et al., G-causality analysis was used to identify the direct functional connectivity between resting-state networks (RSNs) in participants with depression. The study found that subjects with depression had significantly decreased intra-FC within the lateral visual network (VIS), parietal network, and posterior default mode network (DMN); decreased inter-FC between the frontoparietal network (FPN) and subcortical network and between the posterior DMN and anterior DMN; and increased inter-FC between the salience network (SAN) and FPN. Moreover, subjects with depression demonstrated enhanced effective connectivity from the VIS to both the parietal network and cerebellum network.[13]

The G-causality analysis algorithm was used in another study by Zheng et al. to demonstrate that patients with depression show enhanced effective connectivity from the left superior parietal gyrus and superior and middle occipital gyrus to the left hippocampus.[14] Additionally, the G-causality method was used in the investigation of other neuropsychiatric disorders: in a study by Deshpande et al., a classifier for Autism Spectrum Disorder (ASD) was proposed.[15] Furthermore, a study by Haghighat et al. used bivariate G-causality in RSNs for classification of ASD with a maximum accuracy of only 66.66%.[16]

Yu et al. identified seven main networks in a study about connectivity in subjects with depression suffering from childhood trauma. The mentioned networks are as follows: FPN, DMN, dorsal attention network (DAN), sensorimotor network (SMN), SAN, cingulo-opercular network, and VIS. The study reported an increased connection between DMN and FPN, DMN and DAN, as well as between DMN and SAN. Moreover, a decreased connectivity was found between DMN and SAN.[17]

Wavelet decomposition is yet another method that can be used to analyze functional connectivity. Although this method has not yet been used for depression classification and is rather unexplored, there are a couple promising studies suggesting that the wavelet method is worth investigating.

Bernas et al. presented a classifier based on wavelet coherence maps that could be used to analyze fMRI signals in both the time and frequency domains. The coherent patterns or time synchronicities between different network activations could be visualized and used to discriminate between subjects with ASD and neurotypical subjects with a reported accuracy of 86.7%.[18] In a study by Khan et al., wavelet coherence was applied to electroencephalogram signals within the DMN of 30 subjects with depression and 30 healthy controls. The obtained biomarker was used to train a 2-dimensional convolutional neural network that obtained a test accuracy of 98.1% for detecting depression.[19]

A feature selection algorithm is a desirable addition to this study since it is important to identify the most relevant RSN pairs for each classification experiment in order to ensure that the most informative features are selected while minimizing overfitting. For this reason, the Maximum Relevance and Minimum Redundancy (MRMR) algorithm is used. MRMR is an algorithm that aims to identify a small set of features that, when put together, yield the maximum possible predictive power.[20]

In this study, we propose three new features based on the wavelet coherence map as well as using the pairwise conditional G-causality. The RSNs that appear to be abnormal in subjects with depression, as found by previous studies, include the DMN, executive network, SAN, SMN, DAN, FPN, and visual cortex. This constitutes our hypothesis as we expect to identify atypical correlations as well as abnormal dynamical patterns between pairs consisting of these networks that are present in subjects with depression.

For the classification of the subjects with and without depression, two popular classifiers were used: SVM and decision tree. SVM is a supervised discriminative classifier that constructs hyperplanes to separate data into groups using labeled data with which it is trained. The decision tree classifier uses a tree representation of nodes to test several attributes of the data and learn decision rules inferred from the features to predict the label of a target variable. Both classifiers have been successfully applied in neuroimaging studies and are therefore implemented in this study.[21–23]

METHODS

The dataset, containing a total of 72 subjects, was obtained from OpenNeuro.org.[24] The participant selection as well as the image acquisition were performed by Bezmaternykh et al. and the methods are

TABLE 1 Demographic and clinical characteristics of the groups involved in the study

	Control	Depressed
Sex	6 M, 15 F	13 M, 38 F
Age (years)	33.8 ± 8.5	33.1 ± 9.5
IQ	106.0 ± 16.1	103.7 ± 14.6
MADRS	Not applicable	26.7 ± 4.4
BDI	4.6 ± 4.5	20.7 ± 10.0
ZSRDS	32.1 ± 5.9	46.4 ± 7.0

Note: All the data represent mean ± standard deviation unless otherwise indicated.

Abbreviations: BDI, Beck Depression Inventory; F, females; IQ, intelligence quotient; M, males; MADRS, Montgomery-Asberg Depression Rating Scale; ZSRDS, Zung Self-Rating Depression Scale.[30.]

presented in detail in their study.[25] The study involves 51 medication-free patients with a diagnosis of mild depressive episode, moderate depressive episode, or dysthymia according to the International Classification of Diseases 10th Revision, as established in the multiprofile clinic Pretor and International Institute of Psychology and Psychotherapy, Novosibirsk, Russia. The control group consists of 21 healthy control subjects without a psychotic, neurological, or somatic disorder or any MRI contraindication. There is no significant difference between the two groups in terms of gender, age, and intelligence level (Raven's Progressive Matrices test). All subjects signed informed consent to participate in the experiment.[25] Demographic and clinical characteristics of the groups involved in the study are presented in Table 1.

The fMRI scans were obtained using a 3T Ingenia Philips scanner. The following parameters were used to acquire the T2*-weighted single-shot echo planar imaging scans: $2 \times 2 \times 5$ mm spatial resolution, repetition time (TR)/echo time 2500/35 ms, and fat suppression mode. The reference anatomical image was acquired using a T1-weighted 3-dimensional turbo-field echo sequence with a spatial resolution of $1 \times 1 \times 1$ mm. All subjects were instructed to lie still without performing any specific task for a duration of 4 minutes. With a TR of 2.5 seconds, this resulted in 100 volumes per subject.[25]

Data preprocessing is necessary in order to reduce the effects of artifacts, caused by movement and physiological confounders, separate brain tissue from nonbrain tissue such as the skull, as well as bringing all participants scans in the same reference space by registration. The preprocessing of the data was carried out using FMRIB Software Library (FSL) and it consisted of two main stages.[26] In the initial stage, the following set of operations was applied using the MELODIC 3.0 (multivariate exploratory linear optimized decomposition into independent components [ICs]) tool within FSL: motion correction (MCFLIRT), nonbrain tissue removal, slice timing correction, spatial smoothing using a Gaussian kernel of 5.0 mm full width at half-maximum, intensity normalization, and high-pass temporal filtering at 0.01 Hz. Single-session independent component analysis (ICA) was performed on each subject using automatic dimensionality estimation to find components that are of neuronal origin. With ICA, we separate fMRI signal sources in the brain that allows us to find spatially independent, yet coherent brain activation patterns present in the data, resulting in so-called ICs. These can be of neural or nonneural origin.

The denoising stage consisted of classifying and removing noise components that were found by the single-session ICA. The FSLeyes tool within FSL was used to visualize and label each component within the single-session ICA as either signal or noise. The labeling process was performed manually by following the guidelines and methods imposed by Griffanti et al.[27] The removal of noisy components was carried out using the "regfilt" tool within FSL, which applies regression to remove the unwanted components and create a "clean" version of the ICA signal. The reason for manually removing the noisy components from the single-session ICA was to ensure that no useful signal was discarded that could decrease the quality of the data.

Using the denoised signal obtained from the preprocessing stage described above, group ICA is carried out on each subject group: depressed and control. At this stage, one depression subject had to be discarded due to corrupted data and, therefore, the analysis continued with 50 depressed subjects and 21 controls. Group ICA was performed using the MELODIC tool within FSL to find the common components shared by all the subjects within one group. Registration to Montreal Neurological Institute standard space was applied before group ICA.

From the obtained ICs, 10 were selected as RSN based on the Smith et al. RSN atlas.[28] This atlas is established following network analysis of resting-state functional imaging studies with over 30,000 healthy subjects and is therefore a condensation of the most commonly found networks in the brain. The RSNs in this study were selected using a "goodness-of-fit" approach,[18] where the degree of resemblance between each of the IC map and the RSN atlas was calculated. The resulting RSNs were identified based on the highest score obtained as well as by visual inspection to verify and confirm the results obtained in the previous steps. Lastly, dual regression was applied to obtain the RSN spatial maps and time series for each subject separately.[29]

The RSNs selected from the Smith et al. atlas were the following: Primary/Medial Visual Network (VISU1), Lateral Visual (VISU2), Default Mode Network Anterior (DMN1), Default Mode Network Posterior (DMN2), Cerebellum (CEREB), SMN, Auditory Network (AUDI), Executive Network, Frontoparietal Right Network (FPR), Frontoparietal Left Network as well as two additional networks, the Lateral Motor Network (LMN) and DAN.[30,31] Figure 1 is a representation of the 12 identified RSNs that will be used in this study.[28,30,31]

After obtaining the time series from all the RSNs, the wavelet coherence maps and the pair-wise G-causality are computed. All possible permutations of RSN pairs were used (12×12 networks = 144), while removing identical network pairs (e.g., DMN-DMN). This resulted in a total of 132 network pairs.

The wavelet coherence map was obtained for each RSN pair. Three distinct features were extracted from the wavelet coherence map as described in the methodology: total wavelet coherence, wavelet lead coherence, and wavelet coherence blob analysis. Subsequently, pair-wise conditional G-causality was calculated between all RSN pairs using the multivariate G-causality MATLAB toolbox.[32]

For each of the features mentioned above, the feature selection algorithm was employed to rank the most relevant features for

FIGURE 1 The visual representation of the 12 resting-state networks
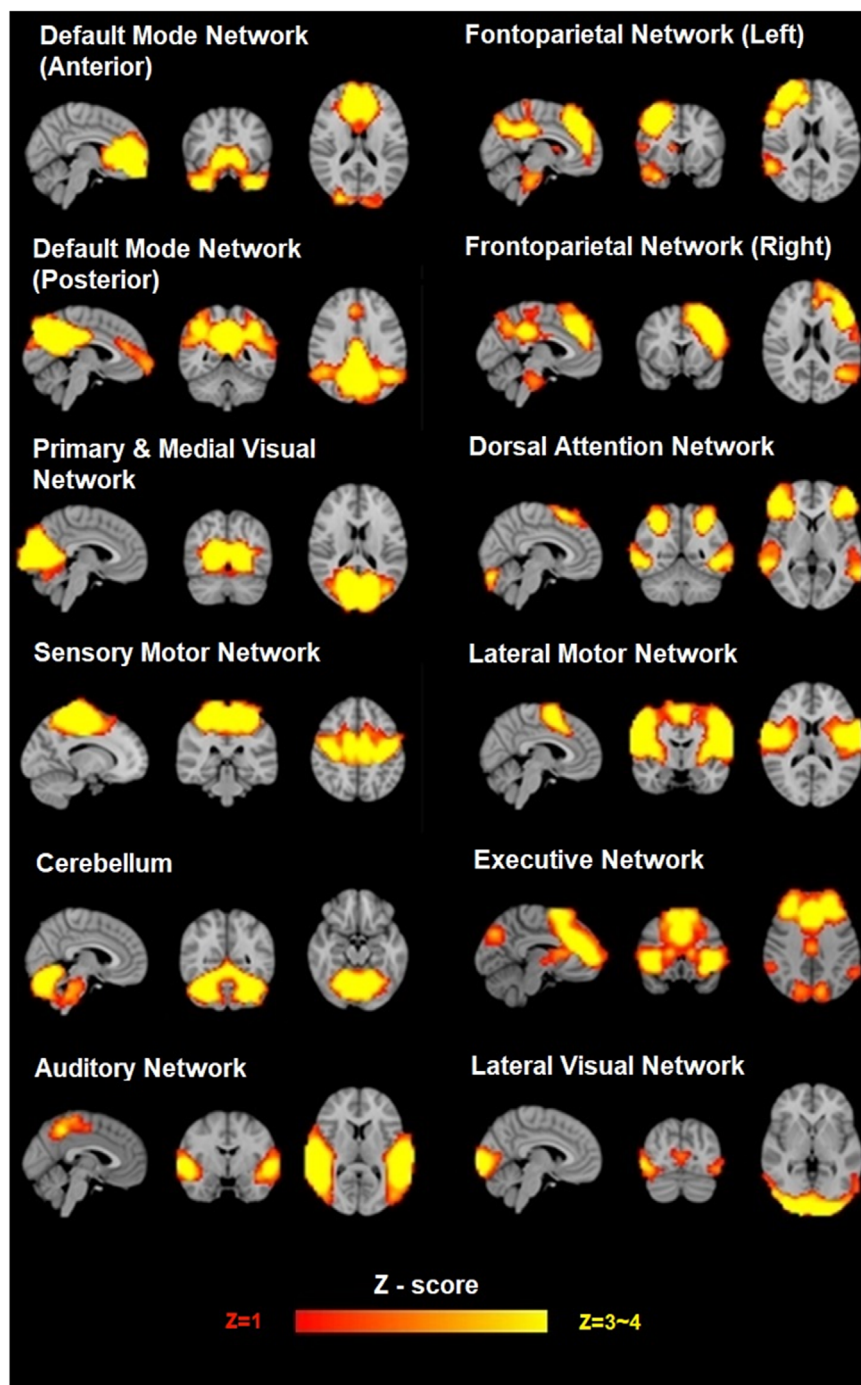
depression classification. Subsequently, an SVM and decision tree classifier were used to classify subjects with and without depression. The classifications were validated using leave-one-out cross-validation.

To compare the results obtained from the experiments with previous findings, a validation session was performed that consisted of the same methods applied on only the RSN pairs that have been found to be abnormal in depression in the literature. A list of 19 RSN pairs between which altered connectivity patterns were found in depression, according to the studies mentioned in the introduction, was compiled. The same feature selection and classification algorithms were used as in the original experiments. Comparisons were made between the results of

the original and literature-based validation feature sets. Figure 2 is a schematic of the methodology of this study, starting from acquisition of the raw fMRI data and ending with the detection of subjects with depression, based on the proposed features.

Wavelet coherence

Wavelet analysis has become a useful tool in seismology studies because it allows the analysis of both time and frequency content in a time series. In other words, the wavelet analysis decomposes the time
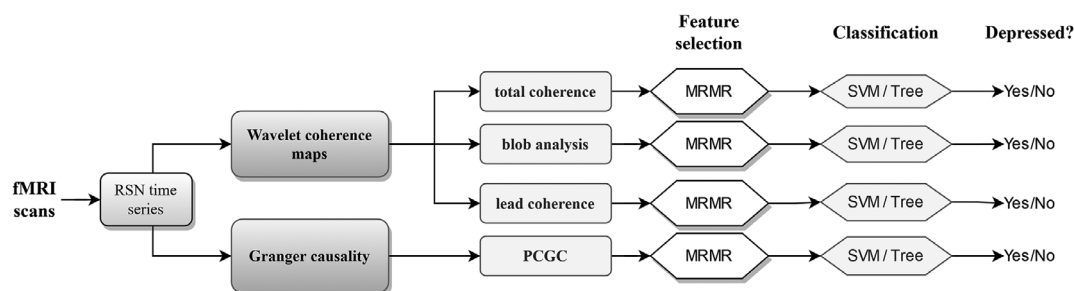
FIGURE 2 Flowchart of the feature extraction and classification process containing the main steps: extraction of RSN time series, analysis of the RSN pair connectivity with wavelet coherence and Granger causality, the extraction of the three wavelet-based features and PCGC feature, feature selection with MRMR, and finally classification using SVM and decision tree classifiers. The classification takes place using each of the four metrics separately and obtains performance scores corresponding to each individual metric. RSN, resting-state network; PCGC, pairwise conditional Granger causality; SVM, support vector machine; MRMR, maximum relevance minimum redundancy
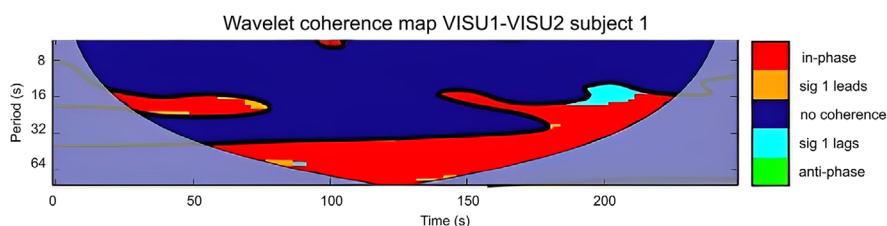

FIGURE 3 Wavelet coherence maps between Primary/Medial Visual Network (VISU1) and Lateral Visual Network (VISU2) of subject 1. The map offers information about the type of coherence present at each time and period. The faded area on the margins of the map represents the cone of influence where edge effects might be present. The color bar shows the type of phasing between signals. s, second; Sig, signal

series into several time blocks to determine the dominant frequency components in a given period.[33]

In this paper, wavelet coherence is used to find out how activation patterns between two network signals interact (synchronous, anticorrelated, causal, or no interaction) within a given time period per frequency. Specifically, the wavelet coherence determines the level of coherence of the cross-wavelet transform of two signals. Based on the cross-wavelet phase, we can deduce a directionality in the coherence between time series (in-phase, antiphase, lead, and lag). This indicates how the brain activation between two networks changes over time for each frequency. Two network time series in-phase are activated synchronously, whereas two time series antiphase might indicate anticorrelated activation. Lead and lag patterns reflect potential causality (one network activates another network or vice versa). A detailed explanation on the construction of wavelet coherence maps can be found in the study by Grinsted et al.[33] We can extract wavelet coherence maps from the RSNs time series by calculating the cross-spectrum between the two signals. In this way, the common power is measured as well as their phase information at various times and scales. Figure 3 is an example of a wavelet coherence map.

Wavelet total coherence

The total wavelet coherence map is calculated by binarizing the obtained wavelet coherence matrices. This binarization step assigns 0s

to elements with no coherence and 1s to any coherence regardless of the type (lead, lag, in-phase, antiphase). Therefore, it reflects the duration and presence of any type of coherence between the activation of two networks. An example of a total wavelet coherence map is visualized in Figure 4A. The total time of coherence is measured by counting the number of elements equal to 1 and averaging over the number of periods in the coherence map ($n = 50$). This feature matrix contains for each participant one number—the total coherence between RSN1 and RSN2—and has the size equal to the number of participants by number of pairs (71×132).

Coherence blob analysis

The coherence blob count reflects the amount of discontinuity in the coherence of activation between RSN1 and RSN2. This can be visualized in Figure 4B. Simply put, this algorithm counts the coherence blobs in the map, and indicates how often the participant switched on and off the coherence between RSN1 and RSN2. This algorithm utilizes a simple blob analysis method, identifying clusters of more than two adjacent nonzero elements in the matrix and counting it as one blob. A blob indicates a period of time in which there is any type of temporal coherence in the activation between two networks, often covering a specific frequency range. This feature matrix contains one number per participant—the number of blobs in the coherence map of RSN1 and RSN2—and has the size equal to the number of participants by number of pairs (71×132).
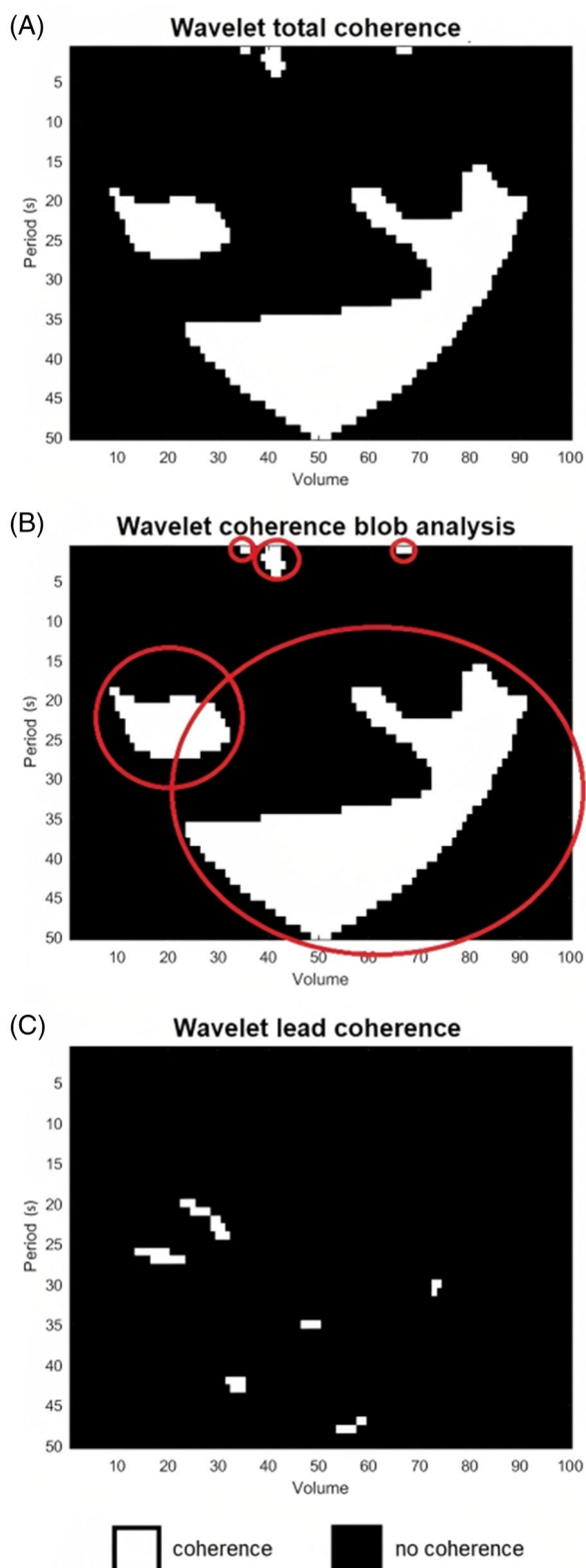
FIGURE 4 (A) Wavelet total coherence map of the RSN pair Primary/Medial Visual Network (VISU1) and Lateral Visual Network (VISU2) for subject 1. (B) Wavelet coherence blob count for the same RSN and subject; each blob of coherence on the map is marked with a red circle. (C) Wavelet lead coherence of the same RSN pair and subject; only the lead coherence type is present, that is, when VISU1 signal leads VISU2. s, second

Wavelet lead coherence

The lead coherence was extracted from the wavelet coherence map obtained in the previous stage (sum of elements indicating a lead of activation of RSN1 with regard to RSN2). This is visualized in Figure 4C. Lead coherence tells us how much time signal X spent leading signal Y and is therefore comparable to the G-causality since it is an indicator that network Y causes X. Wavelet coherence also yields frequency information about the coherence of our signals. In this case, we have obtained 50 separate Fourier periods that we have averaged to simplify the interpretation of the results of this metric. Therefore, for each participant the wavelet lead coherence algorithm counts the time RSN1 leads RSN2 for each period and then averages over all 50 periods to obtain a matrix where each participant is assigned one number—the average lead time between RSN1 and RSN2—and has the size equal to the number of participants by the number of possible pairs (71×132).

Granger causality

The G-causality algorithm used in the analysis of the time series of this study is based on the multivariate G-causality MATLAB toolbox.[32] This toolbox utilizes vector autoregression modeling.

In essence, G-causality is used to find out whether the activation of one RSN is causing the activation of another RSN. By using the aforementioned toolbox, we obtained the G-causality matrix for each subject where each element of the matrix represents a directed pairwise G-causal (PCGC) connection. Since the PCGC matrix contains a causality score for every RSN pair, this matrix is used as a feature vector for the classifiers.

Feature selection and classification

A feature selection algorithm is a desirable addition to this study since it is important to identify the most relevant RSN pairwise connectivity for each classification experiment and aims to prevent overfitting. For this reason, the MRMR algorithm was implemented.[20] MRMR ranks the feature importance by applying each metric separately according to their relevance/redundancy score. This algorithm operates iteratively calculating the factor of the relevance and the redundancy of the feature (relevance/redundancy).[20] With each iteration, the relevance is computed as the F-test between the feature and the target variable, while the redundancy is computed as the Pearson correlation between the feature and all the features previously computed. MRMR is a strict algorithm, selecting only the most valuable features.[20]

Two classifiers were used: an SVM classifier with a polynomial kernel of order 4 and a decision tree classifier.

RESULTS

The classification results discussed in this section can be found in Table 2.

TABLE 2 Performance of classifiers

Wavelet total coherence

	Nr feat	AUC	Accuracy	Sensitivity	Specificity	Precision
SVM	2	.70	75%	33%	92%	67%
Tree	49	.76	80%	67%	86%	67%

Wavelet coherence blob analysis

	Nr feat	AUC	Accuracy	Sensitivity	Specificity	Precision
SVM	2	.75	79%	57%	88%	67%
Tree	3	.84	86%	71%	92%	79%

Wavelet lead coherence

	Nr feat	AUC	Accuracy	Sensitivity	Specificity	Precision
SVM	7	.72	76%	71%	78%	58%
Tree	7	.83	86%	76%	90%	76%

Granger causality

	Nr feat	AUC	Accuracy	Sensitivity	Specificity	Precision
SVM	6	.62	68%	52%	76%	46%
Tree	2	.76	80%	71%	84%	65%

Abbreviations: AUC, area under the curve; Nr feat, number of features; SVM, support vector machine classifier; Tree, decision tree classifier.

The wavelet coherence map

Figure 3 represents an example of a wavelet coherence map obtained from subject 1 (depression) from the VISU1-VISU2 pair. The maps tell us at each period (y-axis) and point in time (x-axis) what coherence type was present. The coherence type is color coded, and it can be either in-phase, antiphase, signal 1 leads, signal 1 lags, or no coherence at all. From Figure 3, it appears that subject 1 exhibits a lot of in-phase coherence between the two networks that suggests that VISU1 and VISU2 are synchronously activated in this case.

Wavelet total coherence

Figure 4A shows an example of a wavelet total coherence map. For this metric, the most informative pairs, according to the MRMR feature selection algorithm, were VISU1-DAN and VISU1-VISU2. An accuracy of 80% and area under the curve (AUC) of .76 was obtained for the decision tree classifier when trained with the values of wavelet total coherence of the top 49 RSN pairs. Figure 5A represents the boxplots of the two most relevant RSN pairs per group and shows that the depression group exhibits more variation and outliers in the average time of total wavelet coherence than the control group. The RSN pairs VISU1-DAN and VISU1-VISU2 are not on the list of most relevant RSN pairs that was ensembled based on the results of previous studies.

Wavelet coherence blob analysis

Figure 4B shows the wavelet coherence map and an illustration of the blob counting process. This metric measures how many times the coherence, independent of coherence type, of the two RSNs activates and deactivates by counting the number of blobs in each map. The best performing RSN pairs according to the MRMR feature selection algorithm were CEREB-LMN and DMN2-AUDI. The highest classification performance was obtained when trained with the blob numbers of three RSN pairs and yielded an accuracy of 86% and an AUC of .84 using the decision tree classifier. From the trends illustrated in the boxplots in Figure 5B, it can be observed that in the case of CEREB-LMN pair, the depression subjects contain more blobs in the wavelet map than the controls. On the other side, the boxplots of the DMN2-AUDI pair show that the depression subjects have less blobs than the controls. The wavelet coherence blob analysis is a novel metric and cannot be directly compared with the literature.

Wavelet lead coherence

The map of the wavelet lead coherence contains only nonzero values for the elements of the coherence map that correspond to the time when RSN1 leads RSN2 and can be seen in Figure 4C. The top selected features for this metric are DAN-AUDI and DMN1-DAN according to the employed feature selection algorithm. The classification accuracy, according to the decision tree classifier and leave-one-out cross-validation, is 86%, while the AUC is .83 when trained with the values of the top seven RSN pairs. This is one of the best performing metrics in terms of accuracy and AUC and matches well with the validation set where the top two most relevant pairs are the same in both experiments. From Figure 5C, we can see that the depression group tends to have higher means and larger ranges for the wavelet lead coherence values than the control group. The depression group also displays more outliers.
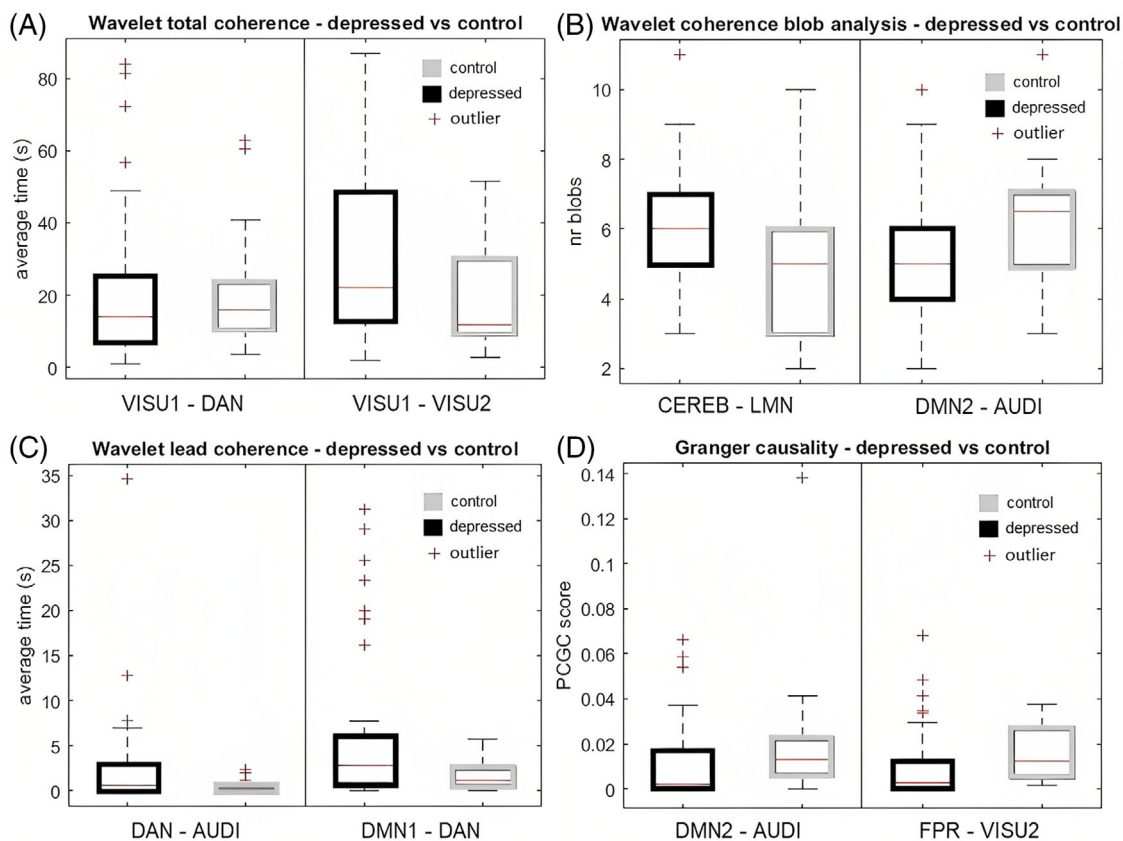
FIGURE 5 Boxplots showing the distributions for each subject group for each metric. (A) Wavelet total coherence—the depressed group exhibits more variation and outliers than the control group. The median for the depressed group is lower than the control in VISU1-DAN, while for VISU1-VISU2 it is higher. (B) Wavelet coherence blob analysis—the pair CEREB-Lateral Motor Network (LMN) shows a higher number of blobs in the depressed group. DMN2-AUDI presents a lower median value for the depressed group. (C) Wavelet lead coherence—the pairs DAN-AUDI and DMN1-DAN present higher variation and medians for the depressed group. (D) Granger causality—the pairs DMN2-AUDI and Right Frontoparietal Network (FPR)-VISU2 show a lower median causality score in depressed subjects. s, second; nr, number; PCGC, pairwise conditional Granger causality

Granger causality

The G-causality top selected RSN pairs consist of DMN2-AUDI and FPR-VISU2. The best classification performance for this metric was obtained using the PCGC values of the two RSN pairs mentioned above and yielded 80% accuracy and .76 AUC. The general trend between groups is illustrated in the boxplots from Figure 5D where it appears that the depression subjects show smaller PCGC values than the control group for both top RSN pairs. Agreement with the literature was found when classifying based on PCGC between the original and validation features as one RSN pair appears in the highest feature importance list for both feature sets (FPR-VISU2).

DISCUSSION

The top performing metrics are wavelet lead coherence and wavelet coherence blob analysis with an accuracy score of over 85%. Figure 6 visualizes the most important interactions between the RSN pairs that have yielded the highest classification scores in predicting depression.

The DMN encompasses multiple brain regions including the anterior medial prefrontal cortex, posterior cingulate cortex, and angular gyrus.[34] It has been found to be responsible of several functions including emotion processing as well as the allocation of attention resources for cognitive processing.[35–36] Many studies show that subjects with depression have an hyperactive DMN as compared to control subjects.[11,13,17,20] These findings correspond with our own results, which show the increased activity between posterior DMN and DAN in subjects with depression when employing the wavelet lead coherence metric.

The DAN is responsible for tasks that require attention to external stimuli and includes the visual motion area, frontal eye fields, superior parietal lobule, intraparietal sulcus, and ventral premotor cortex.[31] In our study, the depression subjects show on average more wavelet lead coherence between the DAN and DMN1 than the control group. This is in accordance with previous studies and suggests that the abnormal interaction between the two brain regions may be responsible for anomalous attention to the external world and internally directed mentation.[36] Hu et al. also found abnormal connectivity within the DMN.[12] These findings are comparable with our results for the wavelet
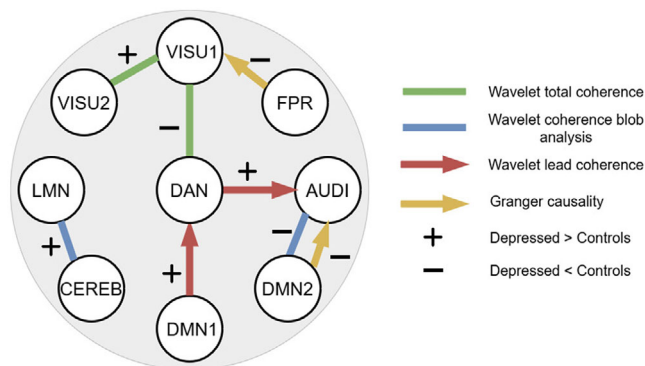
FIGURE 6 Diagram describing the main interactions between RSNs that contributed to the highest performance scores for depression classification. The arrows in wavelet lead coherence and Granger causality represent the importance of direction between RSN pairs. The plus sign shows when the mean value was greater for the depressed group than the control group, while the minus sign shows when the mean value was lower for the depressed group than the controls. The wavelet total coherence and the wavelet coherence blob analysis do not depend on direction. LMN, Lateral Motor Network; VISU1, Primary/Medial Visual Network; VISU2, Lateral Visual Network; FPR, Frontoparietal Right Network

total coherence metric that is decreased between DAN and VISU in participants with depression.

The abnormalities within and between AUDI and VIS have also been linked to depression. Studies show that dysfunctions in these sensory systems, specifically hypoconnectivity, may lead to impaired facial processing, sound processing, and integration of visual and auditory information in subjects with depression.[36–38] In our study, both AUDI and VISU appear frequently in the top selected features of the best performing metrics. Moreover, Yu et al. also discuss the increased connectivity between the FPN and visual system, while in our study the FPR-VISU2 pair showed decreased G-causality scores for the depressed subjects.[17]

One of the best performing metrics utilized in this study is the novel concept of wavelet coherence blob analysis that measures the discontinuity in coherence between RSN pairs. This method is novel and its results are therefore not comparable to any existing literature so far. However, the involvement of the cerebellum and the lateral motor network in depression has been previously documented and linked to cognitive control and emotional processing.[39] In our study, CEREB-LMN is one of the best performing pairs in the blob analysis metric showing more discontinuity on average in the depression group than in the control subjects. This may suggest that in depression subjects, the coherence between the cerebellum and the control network switches on and off more often, while the control subjects maintain the connectivity between the two RSNs for longer periods of time. The literature shows that a significant decrease in motor activity is linked to depression.[40–43] The abnormal co-activation pattern between the cerebellum and the lateral motor network may explain this lack of movement-related activation compared to the control subjects.

The wavelet coherence maps were generated using the Morlet wavelet due to the highest frequency/time resolution ratio. A study compared three popular wavelet types such as PAUL wavelet, a derivative of Gaussian, and Morlet wavelet for the classification of ASD adolescents. They demonstrated that the Morlet wavelet is the most suitable for analyzing neurodynamics, hence our choice for the wavelet type used in the generation of the coherence maps between RSN time series.[44]

The feature selection algorithm is a strength of this study since it provides the opportunity to test all possible RSN pair combinations and select only the most informative pairs while minimizing overfitting. Initially, three feature selection algorithms were tested on a sample of the data: MRMR, chi-squared test, and neighborhood component analysis. Since MRMR outperformed chi-squared test and neighborhood component analysis in almost all situations, we decided to exclude these two algorithms for the other experiments. In the classification phase, four classifiers were initially tested: SVM with a polynomial kernel, SVM with a radial basis function kernel, linear discriminant analysis, and a decision tree. Based on the performance scores obtained using these four classifiers, only two—the SVM with polynomial kernel and the decision tree—were selected.

In some of the cases, the sensitivity of the prediction is quite low (33% for wavelet total coherence SVM) despite high specificity scores. This may be a result from training and testing on an imbalanced dataset, which contained more than double the amount of depression subjects compared to healthy control subjects (50 vs. 21). In this case, the classifier learns and adapts the model for depression quite well due to the larger sample size. Therefore, the model tends to classify more subjects as depression, rather than healthy control. This fact inevitably lowers the overall AUC and decreases the reliability of the results. A good improvement for the future of this study would be to introduce a dataset balancing technique such as undersampling, oversampling, or nested cross-validation.

In terms of future work and limitations of this study, it is important to mention the relatively small sample size of subjects (50 depressed and 21 control) and short acquisition time. As suggestions for future work, a larger and more balanced sample size as well as including more hyperparameter variation in terms of classification and feature selection algorithms is recommended. In addition to this, a longer acquisition time with a shorter TR would benefit this study.

The aim of this study was to develop novel image-based features for the objective diagnosis of depression. We introduced novel highly discriminating features based on wavelet coherence and G-causality that led to depression classification accuracies of 80% and above. These algorithms, being explainable, offered new insights into the role of brain dynamics in depression and therefore have potential of being adopted in clinical practice.

The highest performing metrics involved in depression were the wavelet lead coherence, G-causality, and wavelet coherence blob analysis (86%, 80%, and 86% accuracy, respectively) showing the importance of dynamic features of resting-state activity. The first two metrics measure the amount of causality between brain regions and show that the DMN, DAN, AUDI, VISU, and FPR are heavily involved

in medication-free adults with depression. These RSNs are known to be linked to emotional and attention processing as well as facial and sound processing that can be anomalous in subjects with depression. The third highest performing metric shows abnormal activation patterns between DMN2 and AUDI but also between CEREB and LMN in depression subjects that may be linked to the decreased motor activity.

ACKNOWLEDGEMENTS AND DISCLOSURES

ORCID

Jesper Pilmeyer https://orcid.org/0000-0002-8419-8207
Antoine Bernas https://orcid.org/0000-0002-2006-4891
Jacobus F. A. Jansen https://orcid.org/0000-0002-5271-8060
Marcel Breeuwer https://orcid.org/0000-0003-1822-8970
Albert P. Aldenkamp https://orcid.org/0000-0003-3362-9756
Svitlana Zinger https://orcid.org/0000-0001-9357-3067

REFERENCES

1. Vos T, Abajobir AA, Abate KH, et al. Global, regional, and national incidence, prevalence, and years lived with disability for 328 diseases and injuries for 195 countries, 1990–2016: a systematic analysis for the Global Burden of Disease Study 2016. Lancet. 2017;390:1211-59.
2. American Psychiatric Association A, American Psychiatric Association. Diagnostic and Statistical Manual of Mental Disorders: DSM-5. Washington, DC: American Psychiatric Association; 2013.
3. Goldenberg D, Galván A. The use of functional and effective connectivity techniques to understand the developing brain. Dev Cogn Neurosci. 2015;12:155-64.
4. Friston KJ. Functional and effective connectivity: a review. Brain Connect. 2011;1:13-36
5. Zarghami TS, Friston KJ. Dynamic effective connectivity. Neuroimage. 2020;207:116453
6. Li BJ, Friston K, Mody M, et al. A brain network model for depression: from symptom understanding to disease intervention. CNS Neurosci Ther. 2018;24:1004-19.
7. Brakowski J, Spinelli S, Dörig N, et al. Resting state brain network function in major depression–depression symptomatology, antidepressant treatment effects, future research. J Psychiatr Res. 2017;92:147-59.
8. Chen VC, Chou YS, Tsai YH, et al. Resting-state functional connectivity and brain network abnormalities in depressive patients with suicidal ideation. Brain Topogr. 2021;34:234-44
9. Marchitelli R, Paillère-Martinot ML, Bourvis N, et al. Dynamic functional connectivity in adolescence-onset major depression: relationships with severity and symptom dimensions. Biol Psychiatry Cogn Neurosci Neuroimaging. 2022;7:385-96.
10. Albert KM, Potter GG, Boyd BD, et al. Brain network functional connectivity and cognitive performance in major depressive disorder. J Psychiatric Res. 2019;110:51-6.
11. Sambataro F, Visintin E, Doerig N, et al. Altered dynamics of brain connectivity in major depressive disorder at-rest and during task performance. Psychiatry Res Neuroimaging. 2017;259:1-9.
12. Hu Y, Wen C, Cao G, et al. Brain network connectivity feature extraction using deep learning for Alzheimer's disease classification. Neurosci Lett. 2022;782:136673.
13. Luo L, Wu H, Xu J, et al. Abnormal large-scale resting-state functional networks in drug-free major depressive disorder. Brain Imagin Behav. 2021;15:96-106.
14. Zheng LJ, Yang GF, Zhang XY, et al. Altered amygdala and hippocampus effective connectivity in mild cognitive impairment patients with depression: a resting-state functional MR imaging study with Granger causality analysis. Oncotarget. 2017;8:25021-31
15. Deshpande G, Libero LE, Sreenivasan KR, et al. Identification of neural connectivity signatures of autism using machine learning. Front Hum Neurosci. 2013;7:670.
16. Haghighat H, Mirzarezaee M, Araabi BN, et al. An age-dependent connectivity-based computer aided diagnosis system for autism spectrum disorder using resting-state fMRI. Biomed Signal Process Control. 2022;71:103108
17. Yu M, Linn KA, Shinohara RT, et al. Childhood trauma history is linked to abnormal brain connectivity in major depression. Proc Natl Acad Sci USA. 2019;116:8582-90.
18. Bernas A, Aldenkamp AP, Zinger S. Wavelet coherence-based classifier: a resting-state functional MRI study on neurodynamics in adolescents with high-functioning autism. Comput Methods Programs Biomed. 2018;154:143-51
19. Khan DM, Masroor K, Jailani MF, et al. Development of wavelet coherence EEG as a biomarker for diagnosis of major depressive disorder. IEEE Sens J. 2022;22:4315-25.
20. Peng H, Long F, Ding C. Feature selection based on mutual information criteria of max-dependency, max-relevance, and min-redundancy. IEEE Trans Pattern Anal Mach Intell. 2005;27:1226-38.
21. Yassin W, Nakatani H, Zhu Y, et al. Machine-learning classification using neuroimaging data in schizophrenia, autism, ultra-high risk and first-episode psychosis. Transl Psychiatry. 2020;10:278.
22. Gao S, Calhoun VD, Sui J. Machine learning in major depression: from classification to treatment outcome prediction. CNS Neurosci Ther. 2018;24:1037-52.
23. Orru G, Pettersson-Yeo W, Marquand AF, et al. Using support vector machine to identify imaging biomarkers of neurological and psychiatric disease: a critical review. Neurosci Biobehav Rev. 2012;36:1140-52.
24. Bezmaternykh DD, Melnikov ME, Savelov AA, et al. Resting state with closed eyes for patients with depression and healthy participants. OpenNeuro. Available from: https://openneuro.org/datasets/ds002748/versions/1.0.0. Accessed 13 Dec 2022.
25. Bezmaternykh DD, Melnikov MY, Savelov AA, et al. Brain networks connectivity in mild to moderate depression: resting state fMRI study with implications to nonpharmacological treatment. Neural Plast. 2021;2021:8846097.
26. Jenkinson M, Beckmann CF, Behrens TE, et al. FSL. Neuroimage. 2012;62:782-90
27. Griffanti L, Douaud G, Bijsterbosch J, et al. Hand classification of fMRI ICA noise components. Neuroimage. 2017;154:188-205.
28. Smith SM, Fox PT, Miller KL, et al. Correspondence of the brain's functional architecture during activation and rest. Proc Natl Acad Sci USA. 2009;106:13040-5.
29. Nickerson LD, Smith SM, Öngür D, et al. Using dual regression to investigate network shape and amplitude in functional connectivity analyses. Front Neurosci. 2017;11:115.
30. Oldehinkel M, Mennes M, Marquand A, et al. Altered connectivity between cerebellum, visual, and sensory-motor networks in autism spectrum disorder: results from the EU-AIMS longitudinal European autism project. Biol Psychiatry Cogn Neurosci Neuroimaging. 2019;4:260-70.
31. Vossel S, Geng JJ, Fink GR. Dorsal and ventral attention systems: distinct neural circuits but collaborative roles. Neuroscientist. 2014;20:150-9.
32. Barnett L, Seth AK. The MVGC multivariate Granger causality toolbox: a new approach to Granger-causal inference. J Neurosci Methods. 2014;223:50-68.
33. Grinsted A, Moore JC, Jevrejeva S. Application of the cross wavelet transform and wavelet coherence to geophysical time series. Nonlinear Process Geophys. 2004;11:561-6.

34. Andrews-Hanna JR, Smallwood J, Spreng RN. The default network and self-generated thought: component processes, dynamic control, and clinical relevance. Ann N Y Acad Sci. 2014;1316:29-52.

35. Hamilton JP, Farmer M, Fogelman P, et al. Depressive rumination, the default-mode network, and the dark matter of clinical neuroscience. Biol Psychiatr. 2015;78:224-30.

36. Kaiser RH, Andrews-Hanna JR, Wager TD, et al. Large-scale network dysfunction in major depressive disorder: a meta-analysis of resting-state functional connectivity. JAMA Psychiatry. 2015;72:603-11.

37. Lu F, Cui Q, Huang X, et al. Anomalous intrinsic connectivity within and between visual and auditory networks in major depressive disorder. Prog Neuropsychopharmacol Biol Psychiatry. 2020;100: 109889.

38. Zwanzger P, Zavorotnyy M, Diemer J, et al. Auditory processing in remitted major depression: a long-term follow-up investigation using 3T-fMRI. J Neural Transm. 2012;119:1565-73.

39. Alalade E, Denny K, Potter G, et al. Altered cerebellar-cerebral functional connectivity in geriatric depression. PLoS One. 2011;6: e20035.

40. Chocron O, Aybek S, Paraschiv-Ionescu A, et al. Measuring real life motor activity in depression. J Transl Sci. 2020;7:1-4

41. Finazzi ME, Mesquita ME, Lopes JR, et al. Motor activity and depression severity in adolescent outpatients. Neuropsychobiology. 2010;61:33-40.

42. Sandmeir A, Schoenherr D, Altmann U, et al. Depression severity is related to less gross body movement: a motion energy analysis. Psychopathology. 2021;54:106-12.

43. Tonon AC, Constantino DB, Amando GR, et al. Sleep disturbances, circadian activity and nocturnal light exposure characterize high risk for and current depression in adolescence. Sleep. 2022;45:zsac104.

44. Cîrstian R, Bernas A, Zinger S, et al. Wavelet function evaluation for ASD classification in adolescents based on functional MRI (abstract). Presented at the 8th Dutch Bio-Medical Engineering Conference; January 29, 2021: Egmond aan Zee.